Geoderma 320 (2018) 43–51

Contents lists available at ScienceDirect

Geoderma

journal homepage: www.elsevier.com/locate/geoderma

Soil internal forces initiate aggregate breakdown and splash erosion

Feinan Hu[a,b], Jingfang Liu[c,a], Chenyang Xu[c], Zilong Wang[c,a], Gang Liu[a,b], Hang Li[d], Shiwei Zhao[a,b,c,*]

[a] State Key Laboratory of Soil Erosion and Dryland Farming on the Loess Plateau, Institute of Soil and Water Conservation, Northwest A&F University, Yangling, Shaanxi 712100, China
[b] Institute of Soil and Water Conservation, Chinese Academy of Sciences, Ministry of Water Resources, Yangling, Shaanxi 712100, China
[c] College of Resources and Environment, Northwest A&F University, Yangling, Shaanxi 712100, China
[d] Chongqing Key Laboratory of Soil Multi-Scale Interfacial Process, College of Resources and Environment, Southwest University, Chongqing 400715, China

ARTICLE INFO

Editor: A.B. McBratney

Keywords:
Aggregate stability
Surface potential
Electrostatic force
Slaking effect
Splash erosion

ABSTRACT

Soil erosion is a severe ecological and environmental problem and the main cause of land degradation in many places worldwide. Soil aggregate breakdown is the first key step of splash erosion and is strongly influenced by soil internal forces, including electrostatic, hydration, and van der Waals forces. However, little is known about the influence of soil internal forces on splash erosion. In this study, we demonstrated that both splash erosion rate (SER) and soil aggregate breaking strength (ABS) were significantly affected by soil internal forces. SER and ABS increased first (from 1 to 10^{-2} mol L^{-1}) then became stable (from 10^{-2} to 10^{-4} mol L^{-1}) with decreasing electrolyte concentration in bulk solution. The electrolyte concentration of 10^{-2} mol L^{-1} in bulk solution was the critical point for both soils in splash erosion and soil aggregate stability. The experimental results can be well interpreted by the theoretical analysis of soil internal forces. The surface potential and electric field around soil particles increased with decreasing electrolyte concentration, thereby increasing the electrostatic repulsive force among soil particles. This phenomenon led to soil aggregate breakdown and release of fine soil particles. Soil splash erosion rate and aggregate stability showed a linear relationship ($R^2 = 0.83$). Our results suggest that soil internal forces induce soil aggregate breakdown and then release of fine soil particles when the soil was wetted, supplying the original material for splash erosion. Furthermore, the raindrop impact force is the driving mechanism causing soil particle movement. In summary, splash erosion could be due to the coupling effects of soil internal forces and the raindrop impact force. Our study provides a possible internal controlling method for reducing splash erosion by adjusting soil internal forces between soil particles.

1. Introduction

Soil erosion is the main reason of land degradation and has posed a major threat to many agricultural and environmental safeties (Mhazo et al., 2016; Vaezi and Bahrami, 2014; Ochoa-Cueva et al., 2015). In rain-induced erosion, splash erosion is an important process and the initial step of inter-rill erosion (Legout et al., 2005b; Fernández-Raga et al., 2017). In general, splash process could result in two main consequences: top soil aggregate breakdown and soil fragment movement (Rose et al., 1983; Legout et al., 2005a; Warrington et al., 2009). These phenomena may further affect soil porosity, hydraulic conductivity, surface sealing or crusting, runoff, and soil erosion (Ramos et al., 2003; Falsone et al., 2012; Vaezi et al., 2017; Sachs and Sarah, 2017). Thus, splash erosion is a vital issue that should be considered in soil erosion management and reliable prediction model development.

Splash erosion begins with the breakdown of soil aggregates into small particles (Shainberg et al., 1992; Legout et al., 2005b). In rain-induced erosion, soil aggregate stability mainly depends on changes in rainfall properties (Kinnell, 2005; Ghahramani et al., 2012), such as raindrop shape and size, kinetic energy, intensity, and their various combinations (Jayawardena and Rezaur, 2000; Martinez-Mena et al., 2002; Wei et al., 2007; Pieri et al., 2009; Ziadat and Taimeh, 2013; Fu et al., 2017). Several studies also reported that raindrop force could directly break down soil aggregates and initiate soil erosion (Ekern, 1951; Kinnell, 1990; Van Dijk et al., 2002; Wang et al., 2014). Although rainfall properties are important factors to influence splash erosion, according to the study of Nearing et al. (1987), the raindrop impact pressure was only about 1 to 3 atm. Therefore, it is still not sure whether the raindrop impact force is strong enough that could directly destroy soil aggregate.

* Corresponding author at: No. 26, Xi'nong Road, State Key Laboratory of Soil Erosion and Dryland Farming on the Loess Plateau, Institute of Soil and Water Conservation, Northwest A&F University, Yangling, Shaanxi 712100, China.
E-mail address: swzhao@nwafu.edu.cn (S. Zhao).

https://doi.org/10.1016/j.geoderma.2018.01.019
Received 21 October 2017; Received in revised form 11 January 2018; Accepted 16 January 2018
Available online 04 February 2018

Table 1
Basic physical and chemical properties of soil samples in this study.

Soil type	pH	SOM	CEC	SSA	Particle size distribution		
		($g\,kg^{-1}$)	($cmol_c\,kg^{-1}$)	($m^2\,g^{-1}$)	Clay (%)	Silt (%)	Sand (%)
Loessal soil	8.60	4.6	7.2	23.0	10.6	13.3	76.1
Lou soil	8.01	6.1	23.2	41.5	27.3	41.5	31.2

On the other hand, splash erosion is also affected by soil properties, such as clay content, soil organic carbon, cation exchange capacity, soil water content (Le Bissonnais and Singer, 1992; Le Bissonnais et al., 1995; Wuddivira et al., 2009; Saedi et al., 2016). These soil properties mainly affect soil aggregate stability, which is often employed as an indicator of soil erodibility (Barthès and Roose, 2002; Ramos et al., 2003; Shi et al., 2010). Soil aggregate breakdown during rainfall could be ascribed to slaking, differential clay swelling, and physical–chemical dispersion (Le Bissonnais, 1996; Levy et al., 2003). For soil aggregate stability under a fast wetting process, the mechanisms of soil aggregate breakdown are always ascribed to the slaking effect (Grant and Dexter, 1990; Le Bissonnais, 1996; Zaher and Caron, 2008; Wuddivira et al., 2010). Ramos et al. (2003) investigated the effects of different disaggregation forces on soil aggregate stability and found that most of the studied soils are susceptible to the loss of stability caused by slaking. Wu et al. (2017) reported that slaking is the most disruptive mechanism in aggregate breakdown in soils with the main clay types being kaolinite and illite which were sampled from Central-South China. Slaking is a physical process where soil aggregates are disintegrated either by forces exerted by clay swelling during wetting or by compressed air in aggregate (Zaher and Caron, 2008; Wuddivira et al., 2010). Furthermore, Dinel and Gregorich (1995) found that swelling exerts more effect on aggregates than alterations caused by compressed air during rapid wetting. Clay (e.g. montmorillonite and illite) swelling is mainly due to surface hydration and the overlap of diffused double layer when the clay is immersed into water (Abu-Sharar et al., 1987; Wilson and Wilson, 2014; Hu et al., 2015). The hydration force mainly induces soil aggregate swelling (Hu et al., 2015). Levy et al. (2003) reported that the slaking effect can be affected by soil electrolyte concentration due to their influences on the diffuse double layer. These studies indicated that the slaking effect essentially originated from soil internal forces, especially electrostatic repulsive force and hydration repulsive force, because of the overlap of diffused double layer of colloidal particles.

From the viewpoint of colloidal surface chemistry, soil internal forces, including electrostatic, van der Walls, and hydration forces, considerably affect soil aggregate stability (Farres, 1980; Itami and Fujitani, 2005; Hu et al., 2015; Rengasamy et al., 2016). Among these forces, electrostatic and hydration forces are repulsive forces, inducing soil aggregate breakdown; meanwhile, van der Waals force is an attractive force that restrains aggregate dispersion (Hu et al., 2015). Theoretically, these soil internal forces could produce interparticle pressure as high as 100–1000 atm (Li et al., 2013; Hu et al., 2015); by contrast, raindrop impact pressure is only 1–3 atm (Nearing et al., 1987). Evidently, the raindrop impact force is lower than soil internal forces. Therefore, soil internal forces are more important for soil aggregate stability than raindrop impact force and other factors. Previous studies demonstrated that these soil internal forces are responsible for soil aggregate stability and soil water movement (Hu et al., 2015; Xu et al., 2015; Li et al., 2013; Rengasamy et al., 2016; Yu et al., 2016). However, few works have directly focused on the effect of soil internal forces on splash erosion; future studies on this aspect could improve our knowledge on splash erosion and soil erosion risk prediction.

Here, we hypothesize that soil internal forces could be the initial forces causing aggregate breakdown and subsequent splash erosion due to raindrop impact. Moreover, splash erosion could be due to the coupling effects of soil internal forces and raindrop impact force. Therefore, in this work, we aimed to investigate the influence of soil internal forces on splash erosion, and probe into the background mechanism of rainfall splash erosion.

2. Materials and methods

2.1. Materials

Soil samples were collected from Ansai (109°19′21″E, 36°51′50″N) and Yangling (108°2′30″E, 34°18′14″N) within the Shaanxi Province, which is located in the south of Loess Plateau and is a traditional agricultural planting region in China. Soil erosion in these areas is usually serious in the rainy periods from July to September. The studied soils are Loessal soil and Lou soil, which are developed from loess parent materials and are classified as Calcic Cambisols according to FAO soil classification. Soil texture for Loessal soil and Lou soil are sandy loam and clay loam, respectively. The major crops planted in this region are winter wheat (*Triticum aestivum Linn*) and maize (*Zea mays L.*). For each type of soil, samples were collected from the top 0–20 cm layer of three representative cultivated lands and were then mixed for further use. X-ray diffraction analysis showed that the dominant clay minerals in the two soils were illite (~40%), kaolinite (~20%), chlorite (~20%), montmorillonite (~10%) and vermiculite (~5%). The cation exchange capacity (CEC) and specific surface area (SSA) were measured using the combined method for surface properties determination which proposed by Li et al. (2011); the detailed steps were given in our previous studies (Liu et al., 2013; Tang et al., 2015). The pH, soil organic matter (SOM) and particle size distribution were analyzed using the traditional methods and shown in Table 1.

2.2. Sample preparation

To quantitatively evaluate the effects of soil internal forces on splash erosion and soil aggregate stability, soil samples were saturated by replacing the originally heterogeneous ions adsorbed on the particle surface with specific ion specie, e.g. Na^+. On the other hand, previous studies (Li et al., 2015; Yu et al., 2016) have revealed that Na^+ is a preferable choice to investigate the effects of soil internal forces on aggregate stability due to its weak polarization at the interface of soil colloids. Therefore, Na^+-saturated soil samples were used in the present study. Here, Na^+-saturated soil samples (model aggregates) were prepared following the procedure described by Hu et al. (2015) and Li et al. (2013). In brief, the air-dried soil samples were firstly exchanged with NaCl solution, subsequently washed with deionized water to remove excess Na^+ in the suspension, then oven dried at 60 °C, and finally crushed and sieved to gain model aggregates (1–5 mm in diameter) for the evaluation of splash detachment and aggregate stability.

2.3. Experimental methods

The experiment on raindrop splash erosion was conducted using the combination of rainfall simulator and splash pan. The rainfall simulator was a cylindrical box with an open top. At the bottom of the cylinder, 22 syringe needles with a diameter of 0.6 mm were installed uniformly. During the rainfall, a constant water head was maintained through a hole in the cylinder. The splash pan used was modified according to the

method of Morgan (1978), and also similar with the device shown in Ma et al. (2014). The pan was consisted of collecting and test areas. The collecting area was an inclined plane holder with an outlet connected to the lowest point of the plane. Therefore, we could collect any splashed material from the test area during rainfall simulation. The test area, which was the center of the splash pan, was a circular sieve with a height of 1 cm and a diameter of 10 cm. The size of mesh was 0.25 mm to eliminate from the effect of water film on raindrop impact.

For the splash detachment experiment, Na^+-saturated model aggregates (1–5 mm) were uniformly loaded onto the test area with a bulk density of 1.05 g cm^{-3} according to the volume of circular sieve and the total mass of soil samples in splash pan. The average rainfall intensity was set as 60 mm h^{-1}. The raindrop height was 80 cm, and the average raindrop diameter was 2.5 mm. Different electrolyte concentrations (10^{-4}–1 mol L^{-1}) of NaCl solution were used as rainfall materials to adjust soil internal forces. When the rainfall began, the splashed aggregate fragments were sampled at an interval of 30 s. The experiment was terminated when water film was formed on the surface of the splash pan. The total mass of splashed soil particles was measured. Two replicates were performed for each run.

Soil aggregate stability was represented by soil aggregate breaking strength (w%), which caused by fast wetting and was defined as the mass percentages of fine particles (in diameter of $d < 20$, < 10 and < 5 μm), released from the prepared macroaggregates (1–5 mm) (Le Bissonnais, 1996; Hu et al., 2015). High mass percentage means low stability of soil aggregates and vice versa. Soil aggregate stability was investigated using pipette method as described follow. Specifically, 20 g of Na^+-saturated model aggregates (1–5 mm) were added into a cylinder containing 500 mL of NaCl solution. Soil aggregates broke down immediately when in contact with the electrolyte solution (fast wetting process). After 2 min, the cylinder was shaken slightly and carefully for four times to ensure the even distribution of small particles released into the suspension. The time needed to separate small particles with diameters of < 20, 10, and 5 μm was calculated based on Stokes law. The upper suspension was removed with a siphon when the corresponding time was over. The suspension was dried in an oven, and the mass percentage ($w(< d)$ %, d = 20, 10, or 5 μm) of small particles was determined (Hu et al., 2015; Xu et al., 2015). Based on classic double layer theory, different NaCl concentrations were applied to adjust the electric field around the soil particle surface and the internal forces among the particles. The electrolyte concentration was set as 10^{-4}, 10^{-3}, 10^{-2}, 10^{-1}, or 1 mol L^{-1}.

2.4. Quantitative calculation of soil internal forces

Soil internal forces, including electrostatic, hydration, and Van der Waals forces, can be obtained as showing in our previous studies (Li et al., 2013; Hu et al., 2015). To calculate the electrostatic repulsive force, the surface potential of soil particles under various electrolyte concentrations should be obtained firstly.

The surface potential for 1:1 type electrolyte can be calculated with the following equation (Li et al., 2004):

$$\varphi_0 = -\frac{2RT}{ZF}\ln\left(\frac{1-a}{1+a}\right) \tag{1}$$

$$\frac{\kappa C_T}{Sc_0} = 1 + \frac{4}{1+a} - \frac{4}{1+e^{-1}a} \tag{2}$$

$$\kappa = \sqrt{\frac{8\pi F^2 Z^2 c_0}{\varepsilon RT}} \tag{3}$$

where φ_0 (V) is the particles surface potential, Z is the valence of cation, F (C mol^{-1}) is the Faraday's constant, R (J mol^{-1} K^{-1}) is the gas constant, T (K) is the absolute temperature, c_0 (mol L^{-1}) is the equilibrium concentration of the cation in bulk solution, S (m^2 g^{-1}) is the specific surface area, a is the intermediate variable, ε is the dielectric constant for water, and C_T (mol g^{-1}) is the cation exchange capacity.

The electric field strength around soil particles under different electrolyte concentrations can be calculated using Eq. (4):

$$E(x) = -\sqrt{\frac{8\pi RT}{\varepsilon}\left[c_0\left(e^{-\frac{ZF\varphi(x)}{RT}} - 1\right)\right]} \tag{4}$$

where E(x) is the electric field strength at the distance of x (nm) away from the soil particle surface (V m^{-1}).

Electrostatic repulsive pressure can be calculated using Eq. (5):

$$P_E = \frac{2}{101}RTc_0\left\{\cosh\left[\frac{ZF\phi(d/2)}{RT}\right] - 1\right\} \tag{5}$$

where P_E (atm) is the electrostatic repulsive pressure, d (dm) is the distance between two adjacent particles, and $\varphi(d/2)$ (V) is the potential at the middle of overlapping position of the electric double layers of two adjacent particles, which can be calculated by equation below:

$$\frac{\pi}{2}\left[1 + \left(\frac{1}{2}\right)^2 e^{\frac{2ZF\varphi(d/2)}{RT}} + \left(\frac{3}{8}\right)^2 e^{\frac{4ZF\varphi(d/2)}{RT}}\right] - \arcsin e^{\frac{ZF\varphi_0 - ZF\varphi(d/2)}{2RT}} = \frac{1}{4}d\kappa e^{\frac{-ZF\varphi(d/2)}{2RT}} \tag{6}$$

where κ (1/dm) is the Debye–Hückel parameter; for 1:1 electrolytes, $\kappa = (8\pi F^2 c0 / \varepsilon RT)^{1/2}$.

Van der Waals attractive pressure and hydration repulsive pressure can be estimated by Eqs. (7) and (8), respectively:

$$P_{vdw} = -\frac{A}{0.6\pi}(10d)^{-3} \tag{7}$$

$$P_h = 3.33 \times 10^4 e^{-5.76\times10^9 d} \tag{8}$$

where P_{vdw} (atm) is the van der Waals pressure, and A (J) is the effective Hamaker constant, which is about 5×10^{-20} J in aqueous solution for soil and clay (Li et al., 2013; Hu et al., 2015), P_h (atm) is the surface hydration pressure.

Because both splash erosion rate and soil aggregate breaking strength (w%) are continuous (not discrete) variables of electrolyte concentration, the statistical analysis based on repetition data is often unnecessary (Carrick et al., 2010; Li et al., 2015; Hu et al., 2015). However, here we should emphasize that the repeatability of experimental results must be examined by repetition experiments as did in the present study.

3. Results and discussion

3.1. Splash erosion rate at different electrolyte concentrations

Soil splash erosion rates under different electrolyte concentrations were developed to investigate the effects of soil internal forces on splash erosion. Fig. 1 shows the relationship between splash erosion rate and electrolyte concentration. From this figure it can be seen that, the splash erosion rate first increased as the electrolyte concentration decreased from 1 mol L^{-1} to 10^{-2} mol L^{-1} and then became stable when the electrolyte concentration was further decreased from 10^{-2} mol L^{-1} to 10^{-4} mol L^{-1}. Specifically, the splash erosion rates of both soils approached zero when the electrolyte concentration was 1 mol L^{-1}. When the initial electrolyte concentration was lower than 1 mol L^{-1} but higher than 10^{-2} mol L^{-1}, the splash erosion rate rapidly increased with decreasing electrolyte concentration. For example, the increments of the splash erosion rate from the electrolyte concentration of 1 to 10^{-2} mol L^{-1} were 6.1 and 8.8 g m^{-2} min^{-1} for Loessal soil and Lou soil, respectively. When the electrolyte concentration was lower than 10^{-2} mol L^{-1}, the splash erosion rate did not increase with decreasing electrolyte concentration. The increments of splash erosion rate from the electrolyte concentration of 10^{-2} to 10^{-4} mol L^{-1} were only 0.5 and 1.1 g m^{-2} min^{-1} for Loessal soil and Lou soil, respectively.

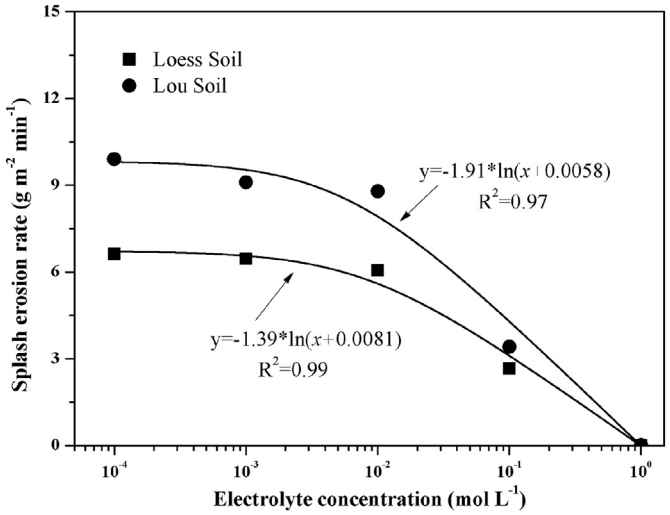

Fig. 1. Relationship between splash erosion rate and electrolyte concentration in bulk solution.

Hence, the electrolyte concentration of 10^{-2} mol L^{-1} was the critical point for soil splash erosion. According to previous studies (Hu et al., 2015; Yu et al., 2017), higher electrolyte concentration in bulk solution corresponded to low net pressure of soil internal forces, and thus more stable soil aggregate; and vice versa. Moreover, when the electrolyte concentrations were lower than the critical point, the net pressures of soil internal forces kept constant, and so did the soil aggregate stability. This indicates that changes of electrolyte concentration would affect soil internal forces among particles, and finally affect aggregate breakdown and splash erosion. The quantitative analyses of soil internal forces are given in detail in the 3.3 section in this work.

The changes in soil splash erosion rate with electrolyte concentration were fitted by logarithmic functions (Fig. 1). The correlation coefficients were satisfactory, with values of 0.99 and 0.97 for Loessal and Lou soils, respectively.

3.2. Soil aggregate stability at different electrolyte concentrations

The first key step of splash erosion is the breakdown of soil aggregate which can supply large amount of fine soil fragments for splash erosion (Shainberg et al., 1992; Legout et al., 2005b). Experiment on soil aggregate stability in various electrolyte concentrations was conducted to investigate the effects of soil internal forces on soil aggregate stability. Soil aggregate stability was characterized by soil aggregate breaking strength (w%), which was evaluated by measuring the mass percentage of fine soil particles (d < 20, < 10 and < 5 μm) released from soil macroaggregates (1–5 mm). Fig. 2 shows the relationship between soil aggregate breaking strength and electrolyte concentration. The soil aggregate breaking strength first increased as the electrolyte concentration decreased from 1 mol L^{-1} to 10^{-2} mol L^{-1} and then became stable when the electrolyte concentration decreased continuously from 10^{-2} mol L^{-1} to 10^{-4} mol L^{-1}. Notably, the electrolyte concentration of approximately 10^{-2} mol L^{-1} was the critical point for soil aggregate stability in both soils. When the electrolyte concentration was lower than the critical point, soil aggregate breaking strength (w%) hardly changed with the decreasing electrolyte concentration. Take w% (d < 10 μm) as an example, the increment of w% (d < 10 μm) from the electrolyte concentration of 10^{-2} to 10^{-4} mol L^{-1} were only 0% and 2.3% for Loessal soil and Lou soil, respectively. However, when the electrolyte concentration was higher than the critical point, w% (d < 10 μm) decreased with increasing electrolyte concentration. The decrements of w% (d < 10 μm) from the electrolyte concentration of 10^{-2} to 1 mol L^{-1} were 7.9% and 12.1% for Loessal soil and Lou soil, respectively. Specifically, there was almost no small particles released from both soils at a high electrolyte concentration of 1 mol L^{-1}, indicating that soil aggregates were relatively stable under this concentration. The changing trends of soil aggregate breaking strength with electrolyte concentration in this work were in line with the previous studies (Hu et al., 2015; Yu et al., 2017). These results could be rationalized by considering the net pressure of soil internal forces (Hu et al., 2015) which will be discussed in 3.3 section of the present work.

Besides, comparison of Figs. 1 and 2 showed similar changing trends in splash erosion rate and soil aggregate stability with electrolyte concentration. This reveals that when a large number of small particles were released, the splash erosion rate was high. Splash erosion and soil aggregate stability exhibited a close relationship.

3.3. Soil internal forces and their distribution around soil particles

According to double layer theory, changes in electrolyte concentration actually affect soil internal forces, and such effect can be quantitatively calculated. To quantitatively analyze the influence of soil internal forces on raindrop splash erosion, in this study we calculated the electrochemical properties of soil particles, electrostatic repulsive force, and net pressure between two adjacent soil particles.

3.3.1. Surface potential and electric field strength

Based on the specific surface area and cation exchange capacity of soils, the surface potential of soil particles at different electrolyte concentration can be quantitatively calculated by the combination of Eqs. (1), (2), and (3), and the results are listed in Table 2. The surface potential (the absolute value) increased with decreasing electrolyte concentration. For example, at a low electrolyte concentration of 10^{-4} mol L^{-1}, the surface potentials of Loessal and Lou soils were 320.2 and 350.0 mV, respectively. At a high electrolyte concentration of 1 mol L^{-1}, the surface potentials were only 94.7 and 120.6 mV for Loessal and Lou soils, respectively. With decreasing electrolyte concentration, the surface potential increased and the soil electric field consequently increased.

Soil particle electric field can be obtained by introducing the surface potential shown in Table 2 into Eq. (4). Fig. 3 illustrates the distribution of the soil electric field around soil particles at different electrolyte concentrations or surface potentials in Loessal and Lou soils. The electric field strength decreased with increasing distance from the particle surface. The soil electric field strength reached approximately -10^8 V m^{-1} at the distance range of 0–2 nm from the particle surface. The operating range of the soil electric field remarkably increased with decreasing electrolyte concentration. For example, when the electrolyte concentration was 10^{-4} mol L^{-1}, the operating range of the soil electric field can exceed 100 nm from the particle surface. However, this range was < 10 nm when the electrolyte concentration in the bulk solution increased by 1 mol L^{-1}.

3.3.2. Electrostatic repulsive pressure and net pressure between soil particles

$\varphi(d/2)$ can be calculated using by introducing the surface potential values shown in Table 2 into Eq. (6) under each electrolyte concentration. By encoding the obtained $\varphi(d/2)$ and the corresponding c_0 value into Eq. (5), we can derive the electrostatic repulsive pressure and its distribution between two adjacent particles in soil aggregates.

Fig. 4 shows the distribution of electrostatic repulsive pressure between two adjacent particle surfaces. The findings are as follows: (1) the electrostatic repulsive pressure decreased with increasing distance between two adjacent particle surfaces; and (2) the electrostatic repulsive pressure between two adjacent particles increased as the electrolyte concentration decreased from 1 to 10^{-2} mol L^{-1} and became stable when the electrolyte concentration was further decreased from 10^{-2} to 10^{-4} mol L^{-1}. For example, at a distance of 2.4 nm between two adjacent particle surfaces of Loessal soil, the electrostatic repulsive pressure increased from approximately 0.21 to 12.7 atm as the electrolyte concentration decreased from 1 to 10^{-2} mol L^{-1}. By contrast,

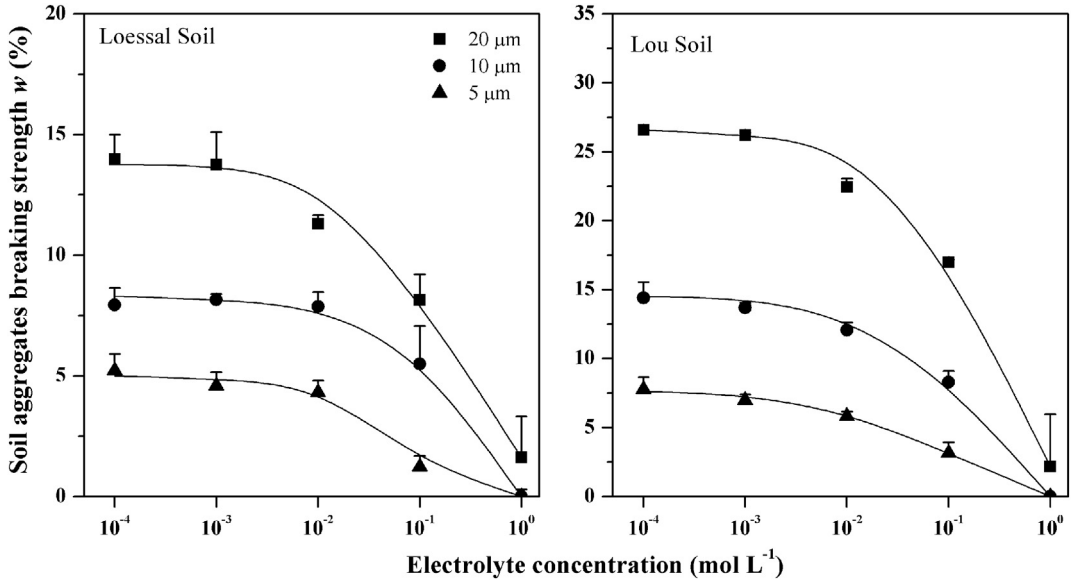

Fig. 2. Relationship between soil aggregates breaking strength and electrolyte concentration in bulk solution.

Table 2
Soil surface potential at different electrolyte concentration.

Electrolyte concentration	Surface potential (mV)	
(mol L^{-1})	Loessal soil	Lou soil
0.0001	−320.2	−350.0
0.001	−261.5	−291.0
0.01	−203.4	−232.5
0.1	−147.2	−175.2
1	−94.7	−120.6

when the electrolyte concentration decreased from 10^{-2} to 10^{-4} mol L^{-1}, the increment in the electrostatic repulsive pressure was only 0.4 atm (from 12.7 to 13.1 atm). A similar trend was also found in Lou soil (Fig. 4). The electrolyte concentration of 10^{-2} mol L^{-1} was the critical point. When the electrolyte concentration was higher than the critical point ($> 10^{-2}$ mol L^{-1}), increase of electrolyte concentration from 10^{-2} to 1 mol L^{-1} would lead to a sharp decrease in electrostatic repulsive pressure. When the electrolyte concentration was lower than the critical point ($< 10^{-2}$ mol L^{-1}), the changes of electrolyte concentration in bulk solution only slightly influenced the electrostatic repulsive pressure. The theoretical results fitted the experimental data shown in Figs. 1 and 2.

The net pressure between two adjacent particle surfaces is the sum of electrostatic repulsive force, van der Waals force, and surface hydration force and can be obtained by applying Eqs. (5)–(8) at the given distance and electrolyte concentration. Fig. 5 shows the distribution of net interaction pressure between two adjacent particle surfaces under different electrolyte concentrations. The results show that: (1) When the distance between two adjacent particles in aqueous solution was < 1.8 nm, strong repulsive pressure was present at any electrolyte concentration, indicating that soil aggregates would only swell under this circumstance. (2) When the distance between two adjacent particles in aqueous solution was 2 nm, the net attractive pressure occurred, with values of −1.7 and −1.3 atm at the electrolyte concentration of 1 mol L^{-1} for Loessal and Lou soils. This finding indicates that soil aggregates would be stable under these conditions. (3) When the electrolyte concentration were < 1 mol L^{-1} for Loessal and Lou soils, the net repulsive pressure was present and increased with decreasing electrolyte concentration. (4) When the electrolyte concentration were $\leq 10^{-2}$ mol L^{-1} for Loessal and Lou soils, the repulsive pressure curves

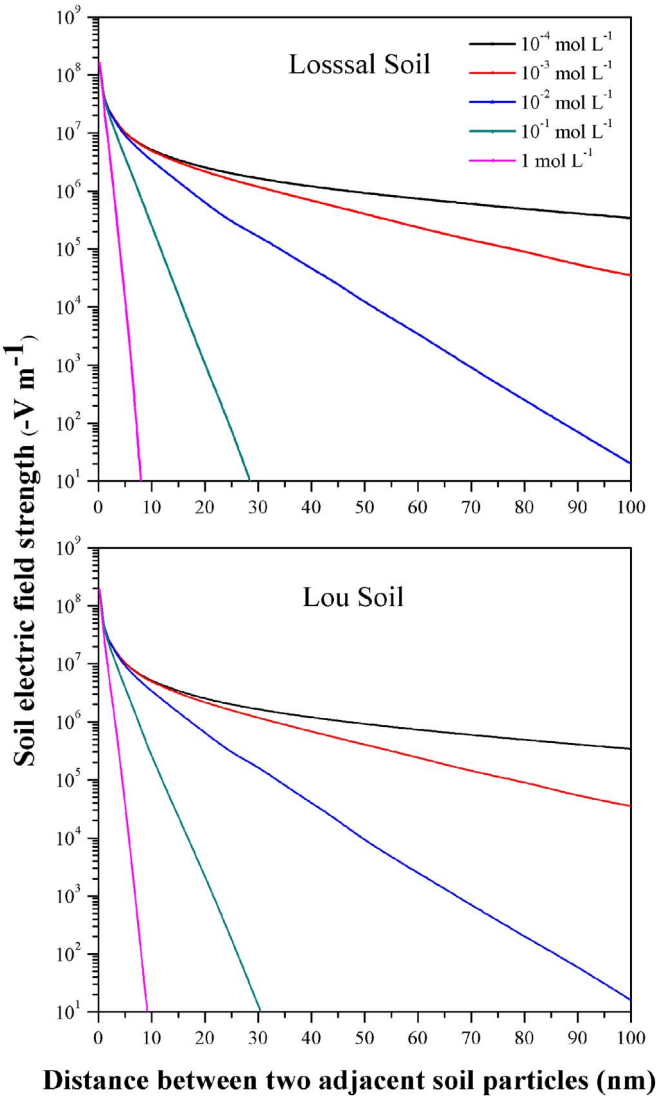

Fig. 3. Distribution of soil electric field around soil particles at different electrolyte concentration.

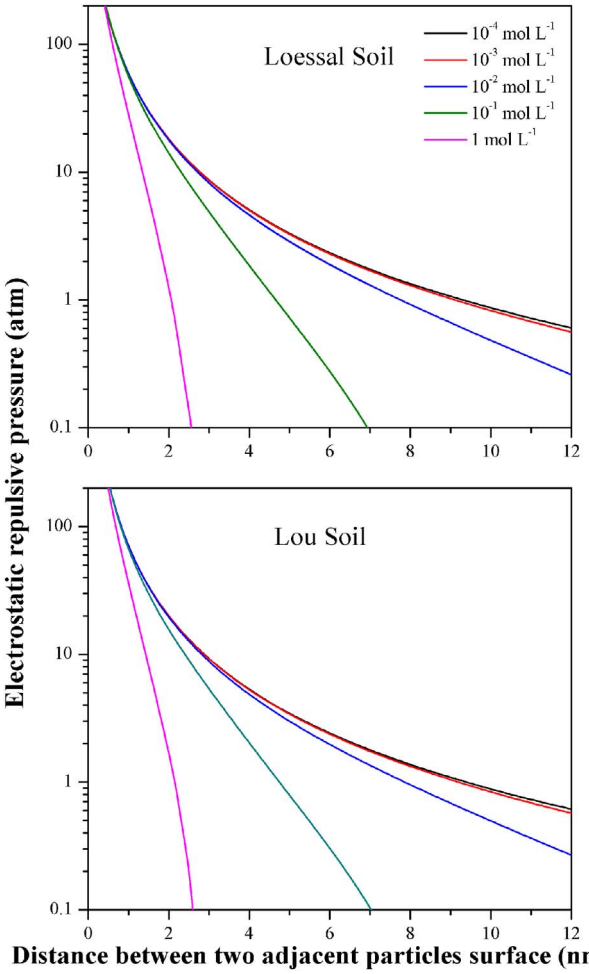

Fig. 4. Distribution of electrostatic repulsive pressure between two adjacent particle surfaces.

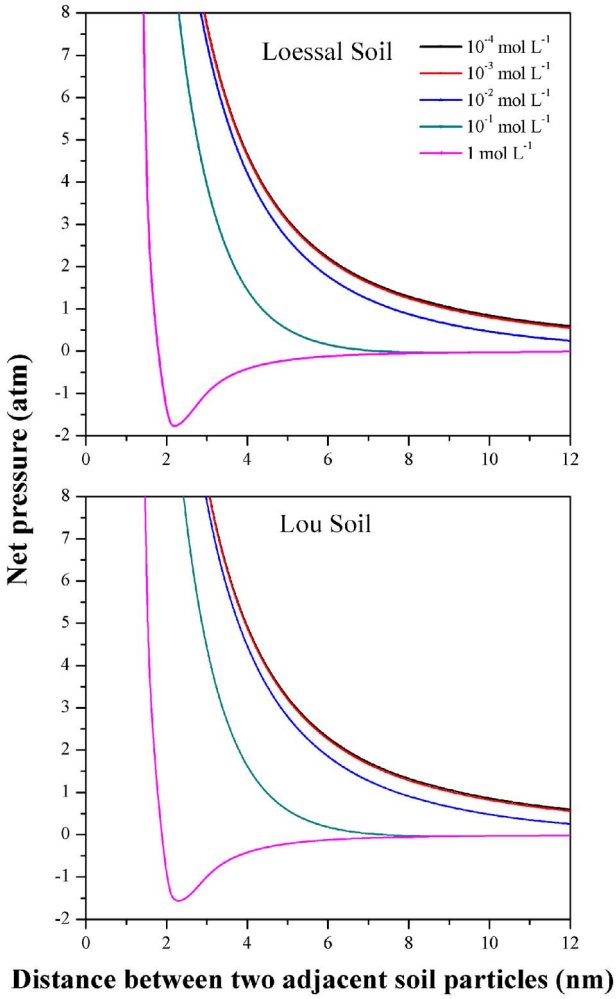

Fig. 5. Distribution of net interaction pressure between two adjacent particle surfaces.

almost overlapped, indicating that these values were the critical electrolyte concentration.

The relationship between the net pressure at the distance of 2 nm between particle surfaces and surface potential was plotted to confirm the changing trends in the net pressure of soil internal forces with soil surface potential. As shown in Fig. 6, the changing trends are similar to those in Figs. 1 and 2. As the surface potential was lower than 203.4 mV for Loessal soil and 232.5 mV for Lou soil, the net pressure between soil particles sharply increased with increasing surface potential. The surface potential of 203 mV was the critical point, which corresponded to the electrolyte concentration of 10^{-2} mol L^{-1}. When the surface potential was higher than the critical point (Fig. 6), the net pressure did not vary with surface potential; as such, the soil aggregate breaking strength will not change. Based on Figs. 1 and 2, the splash erosion rate and aggregate breaking strength did not increase with increasing surface potential or decreasing electrolyte concentration. Thus, the results depicted in Figs. 1, 2, and 6 supported one another. As the surface potential was lower than the critical point, the net pressure sharply increased with increasing surface potential, indicating that the soil aggregate breaking strength will also remarkably increase. This result is consistent with those shown in Figs. 1 and 2. When the surface potentials were 94.7 and 120.6 mV for Loessal and Lou soils, respectively, the net pressure was the attractive one. Under this condition, the soil aggregate stability was rather stable, and nearly no soil fragments (< 20 μm) were splashed. This result is in agreement with those in Figs. 1 and 2. Therefore, the experimental results of splash erosion and soil aggregate stability can be well quantitatively interpreted by considering the variations in soil internal forces at different electrolyte concentrations.

3.4. Effects of soil internal forces on soil aggregate stability and splash erosion

Variations in the electrolyte concentration in bulk solution considerably affect aggregate stability. Specifically, the soil aggregate breaking strength first increased as the electrolyte concentration decreased from 1 to 10^{-2} mol L^{-1} and then became stable when the electrolyte concentration was further decreased from 10^{-2} to 10^{-4} mol L^{-1} (Fig. 2). These results are consistent with previous findings (Abu-Sharar et al., 1987; Hu et al., 2015; Xu et al., 2015; Yu et al., 2017). The variation in the electrolyte concentration in bulk solution mainly affects the soil electrostatic repulsive force, which is responsible for soil aggregate breakdown (Hu et al., 2015). The experimental results in Fig. 2 agree well with the theoretical prediction (Section 3.3), revealing that soil internal forces induce the breakdown of soil aggregates. The present results showed that soil internal forces, including electrostatic, hydration, and van der Waals forces, could reach approximately 100–1000 atm. For example, even though at the distance of 2 nm between two adjacent soil particles, the net pressure is > 15 atm (Fig. 6). Evidently, the pressure produced by compressed air and raindrop impact are lower than that generated by soil internal forces and thus could not directly destroy soil aggregates (Vachaud et al., 1973; Nearing et al., 1987; Zaher et al., 2005; Hu et al., 2015). Soil organic matter, clay content, and soil water content also significantly affect soil

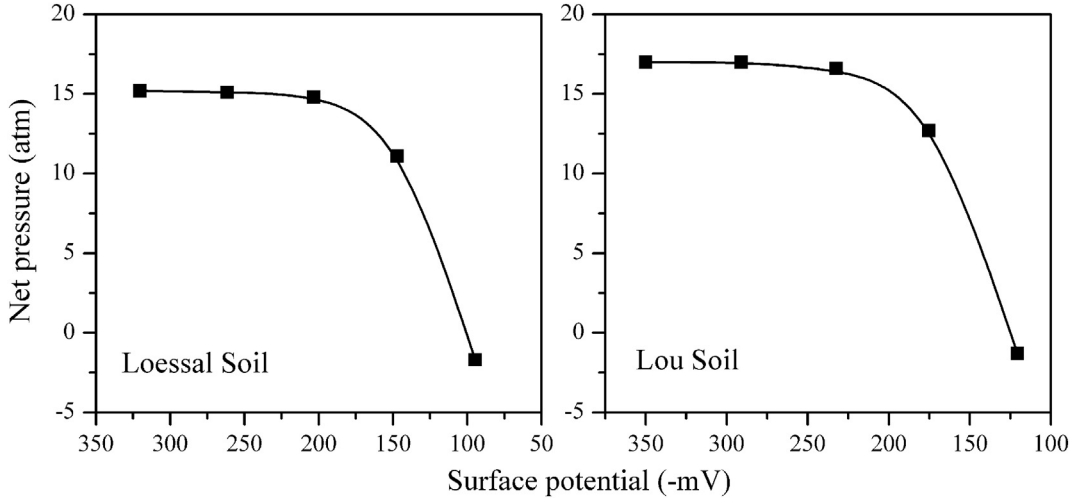

Fig. 6. Relationship between the net pressure at the distance of 2 nm between particle surfaces and surface potential.

aggregate stability. Yu et al. (2017) investigated the coupling effects of soil organic matter and particle interaction forces on soil aggregate stability. They demonstrated that removal of soil organic matter could decrease soil aggregate stability due to the decrease of van der Waals force between soil particles. Wuddivira et al. (2009) reported that both soil aggregate breakdown and splash detachment were affected by the interactive effects of soil organic matter, clay and antecedent moisture contents. However, all these aforementioned factors were constant in the present study. Therefore, the result shown in Fig. 2 cannot be explained by those factors. In conclusion, the results support our hypothesis: it is the soil internal forces initiate soil aggregate breakdown.

Splash erosion begins with the breakdown of soil aggregates into small particles which can supply large amount of fine soil fragments (Shainberg et al., 1992; Legout et al., 2005b). Hence, soil aggregate stability is closely related to splash erosion. Our results showed similar changing trends in splash erosion rate and soil aggregate breaking strength with electrolyte concentration. The soil splash erosion rate and aggregate breaking strength remarkably increased with decreasing electrolyte concentration from 1 to 10^{-2} mol L^{-1} and became stable when the electrolyte concentration decreased from 10^{-2} to 10^{-4} mol L^{-1}. The experimental results in Fig. 1 are in accordance with the theoretical prediction (Section 3.3), showing that soil internal forces could pose important effects on splash erosion. To further assess the relations between soil aggregate stability and splash erosion, we analyzed splash erosion rate and soil aggregate breaking strength ($d < 20$ μm). As shown in Fig. 7, the splash erosion rate is linearly related to soil aggregate breaking strength. This result is consistent with those of other studies (Le Bissonnais, 1996; Barthès and Roose, 2002; Shi et al., 2010; Fernández-Raga et al., 2017), which also reported a good relationship between the parameters of soil aggregate stability and splash erosion. Based on the present results, soil internal forces could induce the soil aggregate breakdown and consequently affect splash erosion.

Generally, the raindrop impact force is the most important factor that can control splash erosion because of the following: (1) the raindrop impact force can directly break up soil aggregates and release large amount of small soil particles; and (2) the raindrop impact force is the only force that can induce the movement of fragments (Fernández-Raga et al., 2017). First, soil internal forces, including electrostatic repulsive, hydration, and Van der Waals forces, could lead to pressure as high as 100–1000 atm; by contrast, the raindrop impact force leads to 1–3 atm only (Nearing et al., 1987). Theoretically, the raindrop impact force is considerably small that it cannot directly break up soil aggregates. Second, if the raindrop impact force plays a decisive role in soil aggregate breakdown, then the splash erosion rate in the present

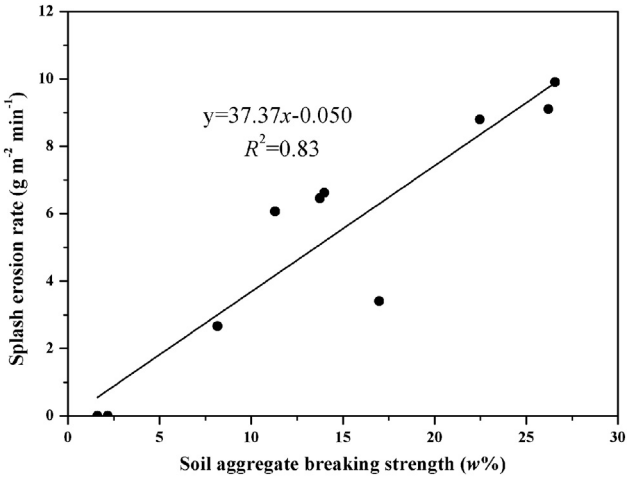

Fig. 7. Relationship between splash erosion rate and soil aggregate breaking strength ($d < 20$ μm)

study should be the same regardless of the electrolyte concentration in the bulk solution. However, the splash erosion rate increased with decreasing electrolyte concentration (Fig. 1). It should be noted that raindrop impact can cause different splash erosion rates due to different raindrop shape, intensity, kinetic energy, etc. (Jayawardena and Rezaur, 2000; Martinez-Mena et al., 2002; Wei et al., 2007; Pieri et al., 2009; Ziadat and Taimeh, 2013; Fu et al., 2017), but the rain intensity and height were constant in our study. Meanwhile, soil aggregates and the experimental procedures used in this study were also identical. On the other hand, according to the results shown in Fig. 2, soil aggregate could also be dispersed without raindrop impact force; this indicates that raindrop impact force is not necessary for soil aggregate breakdown. Finally, it is worthy to point out that, the slaking effect caused by air pressure was also identified as an important factor that affects soil aggregate stability (Ramos et al., 2003; Wu et al., 2017), but the air pressure was < 1 atm (Vachaud et al., 1973; Zaher et al., 2005). In other words, the slaking effect was also not strong enough to result in release of fine soil particles (e.g. < 20 μm) from macro-aggregates in this study (Le Bissonnais, 1996). Therefore, soil internal forces, not the raindrop impact force, can directly induce soil aggregate breakdown. But, on the other hand, soil internal forces are short-range forces (< 50 nm) that cannot induce the movement of soil fragments. By contrast, the raindrop impact force is the only force that can move soil fragments.

Here, we claimed that as rainfall flows into the soil, the bulk

solution becomes diluted; strong hydration repulsive pressure suddenly occurs among soil particles and induces the swelling of aggregates, while electrostatic repulsive forces become established quickly and promote the breakdown of aggregates (Hu et al., 2015). After soil aggregates are broken down due to soil internal forces, fine soil particles are released and supply large amounts of soil materials for splash erosion. Raindrop impact force is the main driving force that initiates the movement of fine soil particles, and soil internal forces (especially hydration and electrostatic repulsive forces) cause soil aggregate breakdown. Hence, our results suggest that splash erosion could be due to the coupling effects of soil internal forces and raindrop impact force. In addition, this study was conducted under a simple condition by using model aggregates. Therefore, further experiments should be conducted on complicated conditions, which are close to the field condition. Notwithstanding its limitation, this study does prove that soil internal forces initiate aggregate breakdown and subsequent splash erosion due to rainfall.

4. Conclusions

Soil internal forces considerably affect splash erosion. The soil aggregate breaking strength first increased and subsequently became stable with decreasing electrolyte concentration in bulk solution. Soil splash erosion rate showed the same trends with that of soil aggregate stability. Theoretical analysis indicated that the electrostatic repulsive force and the net force increased with decreasing electrolyte concentration in bulk solution, leading to soil aggregate breakdown. Moreover, soil aggregate breakdown induced by soil internal forces released large amounts of small particles, which provided the original materials for splash erosion. Furthermore, the raindrop impact force induced movement on soil fragments. We conclude that soil internal forces initiate aggregate breakdown and subsequent splash erosion. Our study suggests that it is possible to control splash erosion through adjusting soil internal forces between particles. The new background mechanism shed light on reliable prediction model development of soil erosion in the future.

Acknowledgements

This work was jointly supported by the National Natural Science Foundation of China (41601236 and 41330852), the CAS “Light of West China” Program (XAB2016B07), the National Science & Technology Supporting Program (2015BCA01B01), the Open Found from the State Key Laboratory of Soil Erosion and Dryland Farming on the Loess Plateau (A314021402-1613), and the Doctoral Start-Up Research Fund of Northwest A&F University (2452016152).

References

Abu-Sharar, T.M., Bingham, F.T., Rhoades, J.D., 1987. Stability of soil aggregates as affected by electrolyte concentration and composition. Soil Sci. Soc. Am. J. 51 (2), 309–314.
Barthès, B., Roose, E., 2002. Aggregate stability as an indicator of soil susceptibility to runoff and erosion: validation at several levels. Catena 47 (2), 133–149.
Carrick, S., Almond, P., Buchan, G., Smith, N., 2010. In situ characterization of hydraulic conductivities of individual soil profile layers during infiltration over long time periods. Eur. J. Soil Sci. 61 (6), 1056–1069.
Dinel, H., Gregorich, E., 1995. Structural stability status as affected by long-term continuous maize and bluegrass sod treatments. Biol. Agric. Hortic. 12 (3), 237–252.
Ekern, P.C., 1951. Raindrop impact as the force initiating soil erosion. Soil Sci. Soc. Am. J. 15 (C), 7–10.
Falsone, G., Bonifacio, E., Zanini, E., 2012. Structure development in aggregates of poorly developed soils through the analysis of the pore system. Catena 95, 169–176.
Farres, P.J., 1980. Some observations on the stability of soil aggregates to raindrop impact. Catena 7 (2–3), 223–231.
Fernández-Raga, M., Palencia, C., Keesstra, S., Jordán, A., 2017. Splash erosion: a review with unanswered questions. Earth Sci. Rev. 171, 463–477.
Fu, Y., Li, G.L., Zheng, T.H., Li, B.Q., Zhang, T., 2017. Splash detachment and transport of loess aggregate fragments by raindrop action. Catena 150, 154–160.
Ghahramani, A., Ishikawa, Y., Mudd, S.M., 2012. Field experiments constraining the probability distribution of particle travel distances during natural rainstorms on different slope gradients. Earth Surf. Process. Landf. 37, 473–485.
Grant, C.D., Dexter, A.R., 1990. Air entrapment and differential swelling as factors in the mellowing of molded soil during rapid wetting. Soil Res. 28 (3), 361–369.
Hu, F.N., Xu, C.Y., Li, H., Li, S., Yu, Z., Li, Y., He, X.H., 2015. Particles interaction forces and their effects on soil aggregates breakdown. Soil Tillage Res. 147, 1–9.
Itami, K., Fujitani, H., 2005. Charge characteristics and related dispersion/flocculation behavior of soil colloids as the cause of turbidity. Colloids Surf. A Physicochem. Eng. Asp. 265 (1), 55–63.
Jayawardena, A.W., Rezaur, R.B., 2000. Drop size distribution and kinetic energy load of rainstorms in Hong Kong. Hydrol. Process. 14 (6), 1069–1082.
Kinnell, P.I.A., 1990. The mechanics of raindrop induced flow transport. Aust. J. Soil Res. 28, 497–516.
Kinnell, P.I.A., 2005. Raindrop-impact-induced erosion processes and prediction: a review. Hydrol. Process. 19 (14), 2815–2844.
Le Bissonnais, Y., 1996. Aggregate stability and assessment of soil crustability and erodibility: I. Theory and methodology. Eur. J. Soil Sci. 47 (4), 425–437.
Le Bissonnais, Y., Singer, M.J., 1992. Crusting, runoff, and erosion response to soil water content and successive rainfalls. Soil Sci. Soc. Am. J. 56 (6), 1898–1903.
Le Bissonnais, Y., Renaux, B., Delouche, H., 1995. Interactions between soil properties and moisture content in crust formation, runoff and interrill erosion from tilled loess soils. Catena 25 (1), 33–46.
Legout, C., Leguedois, S., Le Bissonnais, Y., Malam Issa, O., 2005a. Splash distance and size distributions for various soils. Geoderma 124 (3), 279–292.
Legout, C., Leguedois, S., Le Bissonnais, Y., 2005b. Aggregate breakdown dynamics under rainfall compared with aggregate stability measurements. Eur. J. Soil Sci. 56 (2), 225–238.
Levy, G.J., Mamedov, A.I., Goldstein, D., 2003. Sodicity and water quality effects on slaking of aggregates from semi-arid soils. Soil Sci. 168 (8), 552–562.
Li, H., Qing, C., Wei, S.Q., Jiang, X.J., 2004. An approach to the method for determination of surface potential on solid/liquid interface: theory. J. Colloid Interface Sci. 275 (1), 172–176.
Li, H., Hou, J., Liu, X.M., Li, R., Zhu, H., Wu, L.S., 2011. Combined determination of specific surface area and surface charge properties of charged particles from a single experiment. Soil Sci. Soc. Am. J. 75 (6), 2128–2135.
Li, S., Li, H., Xu, C.Y., Huang, X.Y., Xie, D.T., Ni, J.P., 2013. Particle interaction forces induce soil particle transport during rainfall. Soil Sci. Soc. Am. J. 77 (5), 1563–1571.
Li, S., Li, H., Hu, F.N., Huang, X.Y., Xie, D.T., ... 2015. Effects of strong ionic polarization in the soil electric field on soil particle transport during rainfall. Eur. J. Soil Sci. 66 (5), 921–929.
Liu, X., Li, H., Du, W., Tian, R., Li, R., Jiang, X., 2013. Hofmeister effects on cation exchange equilibrium: quantification of ion exchange selectivity. J. Phys. Chem. C 117 (12), 6245–6251.
Ma, R.M., Li, Z.X., Cai, C.F., Wang, J.G., 2014. The dynamic response of splash erosion to aggregate mechanical breakdown through rainfall simulation events in Ultisols (subtropical China). Catena 121, 279–287.
Martinez-Mena, M., Castillo, V., Albaladejo, J., 2002. Relations between interrill erosion processes and sediment particle size distribution in a semiarid Mediterranean area of SE of Spain. Geomorphology 45 (3–4), 261–275.
Mhazo, N., Chivenge, P., Chaplot, V., 2016. Tillage impact on soil erosion bywater: discrepancies due to climate and soil characteristics. Agric. Ecosyst. Environ. 230, 231–241.
Morgan, R.P.C., 1978. Field studies of rainsplash erosion. Earth Surf. Process. Landf. 3 (3), 295–299.
Nearing, M.A., Bradford, J.M., Holtz, R.D., 1987. Measurement of waterdrop impact pressures on soil surfaces. Soil Sci. Soc. Am. J. 51 (5), 1302–1306.
Ochoa-Cueva, P., Fries, A., Montesinos, P., Rodríguez-Díaz, J.A., Boll, J., 2015. Spatial estimation of soil erosion risk by land-cover change in the Andes of Southern Ecuador. Land Degrad. Dev. 26, 565–573.
Pieri, L., Bittelli, M., Hanuskova, M., Ventura, F., Vicari, A., Pisa, P.R., 2009. Characteristics of eroded sediments from soil under wheat and maize in the North Italian Apennines. Geoderma 154 (1), 20–29.
Ramos, M.C., Nacci, S., Pla, I., 2003. Effect of raindrop impact and its relationship with aggregate stability to different disaggregation forces. Catena 53 (4), 365–376.
Rengasamy, P., Tavakkoli, E., McDonald, G.K., 2016. Exchangeable cations and clay dispersion: net dispersive charge, a new concept for dispersive soil. Eur. J. Soil Sci. 7 (5), 659–665 (6).
Rose, C.W., Williams, J.R., Sander, G.C., Barry, D.A., 1983. A mathematical model of soil erosion and deposition processes: I. Theory for a plane land element. Soil Sci. Soc. Am. J. 47 (5), 991–995.
Sachs, E., Sarah, P., 2017. Effect of raindrop temperatures on soil runoff and erosion in dry and wet soils: a laboratory experiment. Land Degrad. Dev. 28 (5), 1549–1556.
Saedi, T., Shorafa, M., Gorji, M., Khalili Moghadam, B., 2016. Indirect and direct effects of soil properties on soil splash erosion rate in calcareous soils of the central Zagross, Iran: a laboratory study. Geoderma 271, 1–9.
Shainberg, I., Levy, G.J., Rengasamy, P., Frenkel, H., 1992. Aggregate stability and seal formation as affected by drops' impact energy and soil amendments. Soil Sci. 154 (2), 113–119.
Shi, Z.H., Yan, F.L., Li, L., Li, Z.X., Cai, C.F., 2010. Interrill erosion from disturbed and undisturbed samples in relation to topsoil aggregate stability in red soils from subtropical China. Catena 81 (3), 240–248.
Tang, Y., Li, H., Liu, X., Zhu, H., Tian, R., 2015. Unraveling the size distributions of surface properties for purple soil and yellow soil. J. Environ. Sci. 32, 81–89.
Vachaud, G., Vauclin, M., Khanji, D., Wakil, M., 1973. Effects of air pressure on water flow in an unsaturated stratified vertical column of sand. Water Resour. Res. 9 (1), 160–173.
Vaezi, A.R., Bahrami, H.A., 2014. Relationship between soil productivity and erodibility

in rainfed wheat lands in northwestern Iran. J. Agric. Sci. Technol. 16, 1455–1466.
Vaezi, A.R., Ahmadi, M., Cerdà, A., 2017. Contribution of raindrop impact to the change of soil physical properties and water erosion under semi-arid rainfalls. Sci. Total Environ. 583, 382–392.
Van Dijk, A.I.J.M., Bruijnzeel, L.A., Rosewell, C.J., 2002. Rainfall intensity-kinetic energy relationships: a critical literature appraisal. J. Hydrol. 261, 1–23.
Wang, L., Shi, Z.H., Wang, J., Fang, N.F., Wu, G.L., Zhang, H.Y., 2014. Rainfall kinetic energy controlling erosion processes and sediment sorting on steep hillslopes: a case study of clay loam soil from the loess plateau, China. J. Hydrol. 512, 168–176.
Warrington, D.N., Mamedov, A.I., Bhardwaj, A.K., Levy, G.J., 2009. Primary particle size distribution of eroded material affected by degree of aggregate slaking and seal development. Eur. J. Soil Sci. 60 (1), 84–93.
Wei, W., Chen, L., Fu, B., Huang, Z., Wu, D., Gui, L., 2007. The effect of land uses and rainfall regimes on runoff and soil erosion in the semi-arid loess hilly area, China. J. Hydrol. 335 (3), 247–258.
Wilson, M.J., Wilson, L., 2014. Clay mineralogy and shale instability: an alternative conceptual analysis. Clay Miner. 49 (2), 127–145.
Wu, X., Wei, Y., Wang, J., Wang, D., She, L., Wang, J., Cai, C., 2017. Effects of soil physicochemical properties on aggregate stability along a weathering gradient. Catena 156, 205–215.
Wuddivira, M.N., Stone, R.J., Ekwue, E.I., 2009. Clay, organic matter, and wetting effects on splash detachment and aggregate breakdown under intense rainfall. Soil Sci. Soc. Am. J. 73 (1), 226–232.
Wuddivira, M.N., Ekwue, E.I., Stone, R.J., 2010. Modelling slaking sensitivity to assess the degradation potential of humid tropic soils under intense rainfall. Land Degrad. Dev. 21 (1), 48–57.
Xu, C.Y., Yu, Z.H., Li, H., 2015. The coupling effects of electric field and clay mineralogy on clay aggregate stability. J. Soils Sediments 15 (5), 1159–1168.
Yu, Z.H., Liu, X.M., Xu, C.Y., Xiong, X.L., Li, Hang, 2016. Specific ion effects on soil water movement. Soil Tillage Res. 161, 63–70.
Yu, Z., Zhang, J., Zhang, C., Xin, X., Li, H., 2017. The coupling effects of soil organic matter and particle interaction forces on soil aggregate stability. Soil Tillage Res. 174, 251–260.
Zaher, H., Caron, J., 2008. Aggregate slaking during rapid wetting: hydrophobicity and pore occlusion. Can. J. Soil Sci. 88 (1), 85–97.
Zaher, H., Caron, J., Ouaki, B., 2005. Modeling aggregate internal pressure evolution following immersion to quantify mechanisms of structural stability. Soil Sci. Soc. Am. J. 69 (1), 1–12.
Ziadat, F.M., Taimeh, A.Y., 2013. Effect of rainfall intensity, slope, land use and antecedent soil moisture on soil erosion in an arid environment. Land Degrad. Dev. 24 (6), 582–590.